NCAPG promotes proliferation of epithelial ovarian cancer by activating the NF-κB and AKT/mTOR pathways

Sixue Wang
The Second Xiangya Hospital of Central South University
Zeying Li
The Second Xiangya Hospital of Central South University
Mingyu Yi
The Second Xiangya Hospital of Central South University
Li Jiang
The Second Xiangya Hospital of Central South University
Tingting Zhang
The Second Xiangya Hospital of Central South University
Xiaoling Fang (fxlfxl0510@csu.edu.cn)
The Second Xiangya Hospital of Central South University
Xi Wang
The Second Xiangya Hospital of Central South University

Research Article

Keywords: Epithelial ovarian cancer, Bioinformatics, NCAPG, EMT, NF-κB pathway, AKT/mTOR pathway

Posted Date: August 2nd, 2022

DOI: https://doi.org/10.21203/rs.3.rs-1900227/v1

Abstract

Objective

Dysregulation of nonstructural maintenance of chromosome condensin I complex subunit G (NCAPG) in ovarian cancer might be associated with tumor progression, while the mechanistic roles of NCAPG in epithelial ovarian cancer (EOC) are still unclear. In this research, we aimed to elucidate the potential role and molecular basis of NCAPG in EOC.

Methods

We identified differentially expressed genes (DEGs) between EOC and normal tissues based on five Gene Expression Omnibus (GEO) datasets (GSE18520, GSE54388, GSE9891, GSE63885 and GSE40595) and The Cancer Genome Atlas (TCGA) database. A protein–protein interaction (PPI) network was established to evaluate the relationship between the DEGs and to screen hub genes. The expression levels of the hub genes were further validated through the Human Protein Atlas (HPA) databases. Additionally, the prognostic values of the hub genes were evaluated by the Kaplan–Meier plotter. Furthermore, the expression of NCAPG, the most remarkable hub gene in EOC, was examined by qRT–PCR, immunohistochemistry (IHC), and western blotting. A2780 and SKOV3 cell lines were stably transfected with lentivirus to build knockdown and overexpression cell lines. CCK8, clone formation, transwell, and flow cytometry assays were used to evaluate the migratory and proliferation potential of EOC cells. Transcriptome profiling analysis was used to reveal the mechanism by which NCAPG regulated the epithelial-mesenchymal transition (EMT) of EOC. Finally, the mechanistic roles of NCAPG were examined through in vitro and in vivo experiments.

Results

Our findings demonstrated that NCAPG expression was enhanced in EOC tissues compared to normal ovarian tissues and was associated with poor prognosis. NCAPG could facilitate the proliferation, invasion, and migration of EOC cells through the EMT mechanism. Mechanistically, NCAPG could activate the NF-κB and AKT/mTOR pathways to regulate the EMT process of EOC.

Conclusion

Overall, our investigation revealed NCAPG as an important candidate oncogene in EOC. Targeting NCAPG could be a novel treatment with the potential to act as an EOC biomarker.

Introduction

Ovarian cancer (OC) is the most fatal gynecologic malignancy and a common malignant tumor in women. Epithelial ovarian cancer (EOC) accounts for approximately 80% of ovarian cancer cases[1]. Due to the hidden onset and symptoms, 60%-70% of patients are diagnosed late and thus miss the opportunity for radical procedures[2, 3]. Consequently, it is vital to elucidate the pathophysiology of EOC and to discover more sensitive prognostic indicators and more effective therapeutic techniques.

The genomic sequencing and bioinformatics analysis of tumors provide precision medicine with potential molecular therapeutic targets for the treatment of a variety of cancers[4–6]. Nonstructural maintenance of chromosomes condensin I complex subunit G (NCAPG) is responsible for the condensation and stabilization of chromosomes during mitosis and meiosis. Numerous bioinformatics studies have suggested that NCAPG is highly expressed in a variety of tumor tissues and might be associated with a poor prognosis[7]. It has been reported that NCAPG upregulation is associated with poor prognosis of hepatocellular carcinoma (HCC), breast cancer (BC), and gastric cancer[7–9]. In addition, NCAPG was targeted by miR-145-3p, a tumor suppressor, and participated in castration resistance in prostate cancer[10]. However, the mechanism of NCAPG in EOC is unclear. Therefore, based on the aforementioned findings, NCAPG as a tumor-promoting gene may play a crucial role in tumor development, and it is vital to investigate its mechanism and biological function in EOC.

The process known as epithelial-mesenchymal transition (EMT), which refers to the transformation of an epithelial cell into a mesenchymal cell, is an important contributor to the progression of ovarian cancer, such as invasion and migration[7, 11–13]. Presently, there is no study showing that NCAPG participates in the EMT processes of EOC. Aberrant NF-κB activation has been observed in multiple cancer types, such as hepatocellular carcinoma, non-small cell lung cancer, and bladder cancer, and NF-κB signaling plays important roles in multiple biological processes, including the immune response, differentiation, cell proliferation, and migration[14–16]. Elevated expression of the NF-κB has been reported in OC and is associated with the prognosis of this disease[17, 18]. In addition, NF-κB could combine with the regulatory sequence of the vimentin gene promoter to promote Twist expression and induce the EMT process[19, 20]. The AKT/mTOR signaling pathway is frequently dysregulated in malignancies and plays a key role in numerous biological processes, including growth, proliferation, and survival[21, 22]. Current research indicates that the AKT/mTOR pathway is critical for the malignant tumor EMT process[23, 24]. At present, there is no report on whether NCAPG can regulate the NF-κB pathway and AKT/mTOR signaling pathway to participate in the mechanism of ovarian cancer.

Here, we examined the expression of NCAPG and the effect of NCAPG on the phenotype of EOC in vivo and in vitro and found that the NF-κB signaling pathway and AKT/mTOR signaling pathway were modulated by NCAPG. Altogether, these results provide a mechanism by which NCAPG modulates the progression and prognosis of EOC.

Materials And Methods

Gene expression data acquisition

Bulk-sequencing data in count form and the survival information of 379 ovarian cancer patients were downloaded from The Cancer Genome Atlas (TCGA) database (https://portal.gdc.cancer.gov/), while the transcriptome data of 180 normal ovary samples were downloaded from the Genotype-Tissue Expression (GTEx) database (https://gtexportal.org/home/). Moreover, microarray data of 487 ovarian cancer samples and 22 normal ovary samples were downloaded from the Gene Expression Omnibus (GEO) (https://www.ncbi.nlm.nih.gov/geo/) database. Detailed information on the five GEO datasets (GSE18520, GSE54388, GSE9891, GSE63885 and GSE40595) is listed in Table S1[25-29].

Identification of differentially expressed genes (DEGs)

In the GEO cohort, the batch effect among different GEO datasets was removed by the “combat” function of the “sva” package in R software[30]. After batch removal, the data were used to identify the DEGs between ovarian cancer and normal ovarian tissues. In detail, significant DEGs were screened by the “limma” package with |log2foldchange| > 50 and adjusted P value < 0.01[31]. In the other cohort, DEGs were identified by the “DESeq2” package between 379 ovarian cancer (TCGA database) and 180 normal ovary tissues (GTEx database) with |log2foldchange| > 4 and adjusted P value < 0.01. Significant DEGs were identified by taking the intersection of these two cohorts. Subsequently, functional enrichment analyses were conducted by the “clusterProfiler” package[32].

Screening of the core hub genes

First, survival-related DEGs were screened by the random forest method using the “survivalsvm” and “randomForestSRC” packages. Next, a protein–protein interaction (PPI) network was constructed based on these significant prognostic genes by the STRING database (https://cn.string-db.org/). The prognostic values of the core hub genes were further validated by the web-based Kaplan–Meier plotter tool (https://kmplot.com/analysis/), and the protein expression levels of the core hub genes were determined through the Human Protein Atlas (HPA) database (https://www.proteinatlas.org/).

Clinical samples

Paraffin-embedded samples, including 90 EOC and 30 normal ovarian tissues, were obtained from the Second Xiangya Hospital between 2016 and 2018. Thirty fresh EOC and 15 normal ovarian tissues were obtained from the Second Xiangya Hospital between 2019 and 2020. None of these EOC patients underwent chemoradiotherapy, radiotherapy or targeted therapy before surgery. Normal ovarian tissues were collected from adenomyosis or hysteromyoma patients who underwent whole-uterus and double-attachment resection. The study was conducted in accordance with the Declaration of Helsinki and was approved by the Research Ethics Committee of the Second Xiangya Hospital of Central South University.

Immunohistochemistry (IHC)

IHC was performed using streptavidin-peroxidase method kit (ZSGB-BIO, China) according to the manufacturer’s protocol. Before dewaxing, the sections were placed in a 60 °C incubator for 20 min,

deparaffinized in xylene and rehydrated in gradient concentrations of ethanol. Antigen retrieval was performed by heating the sections at 100 °C for 15 minutes in sodium citrate buffer (Wellbiology, China). To block endogenous peroxidase activity, 3% hydrogen peroxide was added to the sections for 15 min in the dark and incubated with 5% goat serum at room temperature for 20 min. Then, the corresponding antibodies were added to the sections and incubated overnight at 4 °C. The antibodies used were as follows: NCAPG (1:200, Proteintech) and Ki-67 (1:1000, Proteintech). After being washed with PBS, the sections were incubated with secondary antibodies for 30 min at 37 °C. Finally, the sections were stained with diaminobenzidine (DAB) and counterstained with hematoxylin. The IHC score was calculated by multiplying the intensity and the percentage scores.

Western blotting

Total proteins of tissues and cells were extracted using RIPA buffer (CST, USA) with proteinase inhibitor cocktail I (Merck, GER) for 20 min at 4 °C and then centrifuged at 15000 × g for 15 min. The supernatants were collected, and the protein concentration was measured using BCA Protein Assay Kit (Beyotime, China) and then diluted with SDS—PAGE Loading Buffer 5x (Cwbio, China). A total of 15 μg of protein was separated by 8% or 10% SDS—PAGE and then electroblotted onto a 0.45 μm PVDF membrane (Millipore, USA). After blocking with 5% fat-free milk or 5% bovine serum albumin for 1.5 h at room temperature, the membranes were incubated with primary antibodies at 4 °C overnight. Next, the membranes were incubated with corresponding secondary antibodies (Proteintech, China) at room temperature for 1 h. Finally, immunoreactive bands were visualized using enhanced chemiluminescence detection reagent (Thermo Fisher Scientific, USA) by Amersham Imager 600 (Cytiva, USA). The antibodies used were as follows: NCAPG (1:2000, Abcam), Vimentin (1:5000, Abcam), GAPDH (1:20000, Proteintech), BCL2 (1:5000, Proteintech), Caspase9 (1:1000, Proteintech), CDK4 (1:5000, Proteintech), CCND1 (1:5000, Proteintech), AKT (1:1000, CST), p-AKT (1:1000, CST), P65 (1:1000, CST), p-P65 (1:1000, CST), mTOR (1:1000, CST), and p-mTOR (1:1000, CST).

RNA extraction and qRT—PCR

Total RNA was isolated from tissues and transfected cells by using RNAiso Plus reagent (Takara, Japan). cDNA was synthesized from 1 μg of total RNA using the Evo M-MLV RT Kit (AG Bio, China). qRT—PCRwas carried out on the LightCycler®96 system (Roche, CH) and used the SYBR® Green Premix Pro Taq HS qPCR Kit (AG Bio, China). The expression of NCAPG was normalized to that of GAPDH. The polymerase chain reaction (PCR) thermal conditions were as follows: initial denaturation at 95 °C for 30 s, followed by 40 cycles of two-step PCR 95 °C for 5 s, 60 °C for 30 s and, finally, 95 °C for 15 s, 65 °C for 1 s, and 95 °C for 1 s for the dissociation curve. The $2^{-\Delta CT}$ method was used to analyze relative gene expression.

Cell culture

The human ovarian cancer cell lines OV90, SKOV3, A2780, and OVCAR3 were obtained from Zhong Qiao Xin Zhou Biotech (Shanghai, China). Cells were cultured in RPMI 1640 (Gibco, USA) medium

supplemented with 10% FBS (BI, USA) and penicillin and streptomycin (Gibco, USA). All cell lines were incubated in an atmosphere of 5% CO_2 at 37 °C.

Cell transfection and lentiviral infection

shRNAs and NC-shRNAs of NCAPG were synthesized by RiboBio (Guangzhou, China). shRNAs and NC-shRNAs were transfected into A2780 cells according to the instructions for the Lipofectamine 2000 reagent (Thermo Fisher Scientific, USA). Western blotting and qRT—PCR assays were used to screen the best knockdown efficiency of the shRNA sequence for constructing lentivirus stable knockdown cell lines. Lentiviruses overexpressing NCAPG (LV-NCAPG) and its negative control (LV-NC), as well as lentiviral-based shRNA targeting NCAPG (LV-shNCAPG) and its negative control (LV-shNC), were purchased from Genechem (Shanghai, China). SKOV3 cells were infected with LV-NCAPG and LV-NC at multiplicity of infection (MOI) 160 and 80, respectively. A2780 cells were infected with LV-shNCAPG and LV-shNC at MOI of 40 and 80, respectively. After transfection for 96 h, SKOV3 and A2780 cells were selected for 1 week with puromycin at 3 μg/ml and 2.5 μg/ml, respectively, to establish stable cell lines.

Cell migration and invasion assays

Cell migration and invasion assays were performed with uncoated and Matrigel-coated (BD, USA) Transwell chambers (Corning, USA) with an 8 μM pore size. The stable cell lines ($2x10^4$/well) were suspended in 200 μl serum-free medium and seeded into the upper chambers, and 700 μl 10% FBS medium was added into the lower chambers. After 48 h of incubation, the cells on the lower side of the chambers were fixed with 4% paraformaldehyde and stained with 0.5% crystal violet (Beyotime, China). Migrated or invaded cells were photographed and counted under a light microscope at 20x magnification.

Cell proliferation, cell cycle and apoptosis analysis

Cells ($2x10^3$/well) were seeded into 96-well plates. At 0, 24, 48, 72 and 96 h, 10% CCK8 was added and incubated for 1 h, and then the absorbance was measured at 450 nm. For the colony formation assay, a total of $1x10^3$ cells/well was seeded into 6-well plates and cultured for 14 days in 10% FBS medium at 37 °C. The colonies were fixed with 4% paraformaldehyde and stained with 0.5% crystal violet (Beyotime, China). For apoptosis analysis, cells ($1x10^6$/ml) from different treatment groups were digested with trypsin without EDTA, washed with ice-cold PBS, and centrifuged at 2000×rpm for 5 min, followed by resuspension in binding buffer. Subsequently, the cells were incubated with Annexin-V and PI (Solarbio, China) for 25 min at 4 °C in the dark. Then, the stained cells were analyzed using DxP Athena™ (Cytek Biosciences, USA), and the percentage of Annexin V+ PI- and Annexin V+ PI+ cells was calculated as the apoptosis rate. For cell cycle analysis, 70% icy ethanol was used for cell fixation at 4 °C overnight. After staining with propidium iodide (PI) (Solarbio) and RNase (Invitrogen), the percentage of cells in G1, G2, and S phases was analyzed by DxP Athena™ (Cytek Biosciences, USA).

In vivo experiments

Four-week-old NOD/SCID mice were obtained from SJA Laboratory Animals (Hunan, China). SKOV3 or A2780 cells infected with the indicated lentiviral vectors were suspended in 100 μl mixed liquid PBS and Matrigel and subcutaneously injected into the right armpit of NOD/SCID mice at the age of 5 weeks. After 28 days, the animals were sacrificed and used for measurement and immunohistochemistry staining. The tumor volume was calculated using the following formula: V (mm^3) = 0.5 × length (mm) × $width^2$ (mm^2).

RNA-seq and bioinformatic analysis

Total RNA was isolated from A2780 cells after infection with shNC and shNCAPG virus using RNAiso Plus reagent (Takara, Japan). RNA libraries were prepared according to the manufacturer's instructions for the TruSeq RNA Sample Prep Kit (Illumina, USA). HISAT2 software was used to map all clean reads of mRNA to the UCSC hg38 primary assembly genome. Differential gene expression analysis and bioinformatics analysis were conducted in R. DEGs between the samples were identified using the Bioconductor package DESeq2. We considered a gene differentially expressed when it met the thresholds of |log2 Fold change| ≥ 1.5 and $p < 0.05$. Subsequently, functional enrichment analyses were conducted by Metascape (https://metascape.org/) and Gene Set Enrichment Analysis (GSEA) (www.gsea-msigdb.org).

Statistical analysis

The 2-tailed Student t test was used for comparisons between two groups, and one-way analysis of variance (ANOVA) was used for multiple-group comparisons. Data were plotted using GraphPad Prism 6.0 software. Statistical analyses were carried out with SPSS software. Correlations were analyzed by Pearson correlation. $P < 0.05$ was considered significant.

Results

Identification of DEGs and functional enrichment analyses

After batch effects were removed (Fig. 1A, B), a total of 2388 and 3458 DEGs from the GEO and TCGA-GTEx cohorts were identified by differential analysis (Fig. 1C, D). At the intersection of these two cohorts, 272 significant DEGs were identified, including 240 upregulated genes and 32 downregulated genes (Table S2). Subsequently, functional enrichment analyses were conducted based on these 272 significant DEGs. The results of biological process (BP) analysis revealed that DEGs were enriched in chromosome segregation, nuclear division, organelle fission, etc. DEGs were also enriched in cellular components (CC), including spindles, kinetochores, centromeric regions, etc., as well as in molecular function (MF), including kinetochore activity, serine-type peptidase activity, and microtube motor activity (Fig. 1E). KEGG analysis results suggested that DEGs were enriched in the cell cycle, tight junction, p53 signaling pathway, cell adhesion, etc. (Fig. 1F).

Screening of the core hub genes

After screening by the random forest method, 98 prognostic genes were identified for further analysis (Table S2). As revealed by the results of the PPI network, four core genes were recognized as hub genes, including CDCA5, NCAPG, PBK and TK1 (Fig. 2A, B). The prognostic values of these four hub genes were further validated by the Kaplan–Meier plotter (Fig. 2C-F). As shown by the results of immunohistochemistry from the HPA database, the protein expression level of CDCA5 was lower in OC tumor tissue than in normal ovarian tissue (Fig. 2G), which was not consistent with the results at the mRNA level. In addition, the protein expression level of NCAPG was significantly higher in OC tissue (Fig. 2H), while PBK and TK1 were only slightly
more highly expressed in OC tissue (Fig. 2I, J).

The expression levels of NCAPG were upregulated in EOC clinical samples

Based on the results of bioinformatics analysis, we further validated the expression level of NCAPG in clinical samples. IHC was used to perform a localization and semiquantitative investigation of NCAPG. We found that NCAPG was primarily localized in the cytoplasm and that its expression was higher in 90 EOC tissues than in 30 normal ovarian epithelial tissues. (Fig. 3A, B). We further correlated NCAPG expression with the clinicopathological features of 90 EOC tissues. As shown in Table 1, the intensity of NCAPG staining was significantly associated with the histological subtype (serous), higher tumor grade (G2/3), and advanced stage (FIGO III/IV). Furthermore, the protein expression of NCAPG was higher in the EOC samples than in the normal ovary tissues (Fig. 3C, D), and the increased mRNA expression of NCAPG was also identified to be elevated in the EOC samples (Fig. 3E). Combined with the higher expression of NCAPG being significantly correlated with the poor prognosis, we speculated that NCAPG might be activated and play an important role in the development of EOC.

NCAPG promotes biological behavior, proliferation, and EMT in EOC

To understand the molecular function of NCAPG in EOC cells, the protein and mRNA expression of NCAPG in EOC cell lines (OV90, SKOV3, A2780 and OVCAR3) was detected by western blotting and qRT–PCR. The results revealed that NCAPG was expressed at high levels in OV90 and A2780 cells, moderate amounts in OVCAR3 cells, and low levels in SKOV3 cells (Fig. 4A, B). Next, we chose SKOV3 and A2780 for further study. Short hairpin RNAs (sh1, sh2 and sh3) were used to knockdown NCAPG expression, and the efficiency of knockdown was identified by western blotting and qRT–PCR (Fig. 4C, D). We constructed stable overexpression or knockdown (sh3) of NCAPG by lentivirus in SKOV3 and A2780 cells and used western blotting, qRT–PCR, and FITC 495/519 staining (green) to evaluate the efficiency (Fig. 4E-G). To explore the effect of NCAPG expression on the proliferation of SKOV3 and A2780 cells, CCK8 and clone formation assays were used to investigate cell proliferation. The results showed enhanced proliferation of SKOV3 cells overexpressing NCAPG and reduced proliferation of A2780 cells with NCAPG knockdown (Fig. 4H-J). We next explored the role of NCAPG in cell migration and invasion. In transwell assays with or without Matrigel, we found that SKOV3 cells had a significantly increased ability to migrate or invade when NCAPG was overexpressed and a significantly reduced ability to migrate or invade when NCAPG was knocked down (Fig. 4K-N). Moreover, flow cytometry analysis was used to explore the effect of

NCAPG on apoptosis in EOC cells. NCAPG overexpression resulted in remarkable apoptosis resistance compared with control cells, and apoptosis was increased when NCAPG was knocked down (Fig. 4O, P). Furthermore, we detected the expression levels of apoptosis-related proteins by western blotting. Our results showed that BCL2, which promotes cell survival, was increased substantially, while caspase9, an apoptogenic factor, was significantly decreased upon NCAPG overexpression (Fig. 4Q). The flow cytometry analysis was used to explore the effect of NCAPG on cell cycle in EOC cells. The cell cycle was obviously arrested in G0/G1 phase after NCAPG knockdown (Fig. 4R-U). Since cyclin CCND1 and cyclin-dependent kinases, including CDK4, are involved in cell cycle regulation in G1 phase, we evaluated the expression of these proteins in NCAPG-overexpressing or NCAPG-knockdown cells. Our western blot results showed that CDK4 and CCND1 were decreased upon NCAPG overexpression and enhanced upon NCAPG knockdown (Fig. 4V). In addition, NCAPG knockdown significantly induced E-cadherin, whereas inhibiting vimentin levels and NCAPG overexpression had the opposite effect (Fig. 4W).

NCAPG promotes EMT by activating the NF-κB and AKT/mTOR pathways

To further explore the underlying mechanisms of NCAPG in EOC, we performed genome-wide RNA sequencing (RNA-seq) analysis by NCAPG knockdown in A2780 cells. The results showed that there were 360 DEGs caused by NCAPG knockdown ($|\log2 \text{ Fold change}| \geq 1.5$ and $p < 0.05$), including 234 upregulated genes and 126 downregulated genes (Fig. 5A-B). Functional annotation showed that DEGs were enriched in protein kinase B signaling and NF-κB signaling (Fig. 5C-D). These genes were enriched in the NF-κB pathway and mTOR pathway, according to the results of GSEA (Fig. 5E-F). Based on the above enrichment results, we speculated that NCAPG plays an important regulatory role in EOC progression. Additionally, we detected the enriched signaling pathway through western blotting, and the results showed that depletion of NCAPG inhibited the expression of p-P65, p-AKT, and p-mTOR in A2780 cells (Fig. 5G). In contrast, when NCAPG was overexpressed, the expression levels of the aforementioned signaling pathway proteins were noticeably elevated (Fig. 5G).

NCAPG promotes EOC growth in vivo by activating the NF-κB and AKT/mTOR pathways

To investigate the role of NCAPG in EOC in vivo, we selected immunodeficient nude mice to build xenograft tumor models. Lentivirus-mediated NCAPG knockdown or overexpression and the respective control in A2780 and SKOV3 cells were subcutaneously injected into the right back of NOD SCID mice. The volume of xenograft tumors from mice with NCAPG overexpression was markedly increased compared with that in the control group (Fig. 6A-B). In contrast, the volume of xenograft tumors was significantly decreased when NCAPG was knocked down (Fig. 6C-D). Furthermore, immunohistochemical detection showed that the expression of the proliferation protein Ki-67 was higher in NCAPG-overexpressing cells than in control cells. However, knockdown of NCAPG reduced the Ki-67 level compared with the control (Fig. 6E-F). Additionally, we detected the expression of signaling pathways that had been identified in cell lines in xenograft tumors from mice by western blotting. Our results showed that depletion of NCAPG inhibited the expression of p-P65, p-AKT, and p-mTOR in A2780 cells (Fig. 6G). In contrast, the expression levels of the signaling pathway proteins mentioned above were significantly

increased when NCAPG was overexpressed (Fig. 6H). Taken together, our results demonstrate that NCAPG promotes cell migration, invasion and proliferation by activating the NF-κB and AKT/mTOR pathways.

Discussion

Poor prognosis and aggressive tumor development are frequent characteristics of ovarian cancer. Furthermore, almost 70% of ovarian cancer patients experience tumor relapse, and some patients develop acquired drug resistance to chemotherapy[2–4]. The pathophysiology and etiology of this disease remain less studied despite extensive research conducted over the past 20 years[1, 2, 33]. It is unclear how EOC affects prognosis, tumor relapse, and the emergence of acquired treatment resistance.

The emergence of high-throughput sequencing technology has made combined multiomics data analysis a viable tool for comprehensively clarifying disease heterogeneity, predicting prognosis, and discovering new treatment targets[4, 7]. Several studies on NCAPG have suggested that NCAPG plays the role of a tumor promoter in the development of multiple tumors, such as HCC, breast cancer, lung cancer, and ovarian cancer[7, 9, 34]. Moreover, our study not only detected the protein and mRNA expression of NCAPG in our clinical samples but also connected the NCAPG expression level with the clinicopathological features of EOC for the first time. Our data showed that the expression level of NCAPG was significantly increased in EOC samples, inversely correlated with the degree of differentiation and positively correlated with the stage in EOC. Previous studies have suggested that NCAPG may promote the growth, metastasis, and recurrence of HCC. Additionally, upregulated NCAPG was strongly connected with both BC's poor survival and cell proliferation as well as poor disease-free survival and advanced clinical stage in castration-resistant prostate cancer. In our study, we detected the expression of NCAPG in multiple EOC cell lines, and suitable cell lines were selected for stable transfection by lentivirus and further investigation. Our research has consistently shown that NCAPG overexpression promotes the proliferation, migration, and invasion of EOC cell lines. Hence, we speculated that NCAPG might be crucial in the development of EOC.

The transformation of epithelial cells into mesenchymal cells is crucial to the invasion and metastasis of ovarian cancer[23, 35, 36]. There is currently no study showing that NCAPG participates in the EOC-related EMT process. Overexpression of NCAPG, according to our findings, could significantly increase the EMT process associated with EOC. Therefore, we hypothesize that NCAPG may promote the proliferation, migration, and invasion of EOC cells via an EMT mechanism. Next, we delve deeper into the mechanisms through which NCAPG regulates EOC-related EMT processes. In cancer, the NF-κB pathway is linked to the inflammatory response and other cellular processes, such as EMT and metastasis, and NF-κB activation tends to increase the aggressiveness and metastatic potential of numerous cancers. mTOR is a downstream mediator of the PI3K/AKT signaling pathways that regulates several cellular activities, including cell growth, proliferation, survival, and metabolism, by integrating a range of extracellular and intracellular signals in tumors[24, 37, 38]. It has been reported that the NF-κB pathway and AKT/mTOR are involved in EMT, which is associated with tumors such as gastric cancer, HCC, and EOC[11, 20, 39,

40]. However, there is no report that NCAPG can modulate the aforementioned signaling pathways to engage in EMT of EOC. After NCAPG knockdown, we performed RNA-seq and analyzed the data by GO functional enrichment and GSEA. Following NCAPG knockdown, we found that these genes were enriched in the aforementioned signaling pathways, and western blot analysis revealed that NCAPG overexpression might activate these signaling pathways. Our results suggest that NCAPG promotes EMT, migration, and invasion of EOC cells by activating the NF-κB and AKT/mTOR pathways.

Conclusion

In conclusion, our results showed that NCAPG could promote the invasion, migration, and proliferation of EOC cells by activating the NF-κB and AKT/mTOR pathways in EMT of EOC. This investigation identified NCAPG as a clinically important target that is essential for EOC cell proliferation. Targeting NCAPG may be a novel therapy with the potential to serve as a predictive biomarker for EOC.

Abbreviations

OC, ovarian cancer; EOC, Epithelial ovarian cancer; NCAPG, Nonstructural maintenance of chromosomes condensin I complex subunit G; HCC, hepatocellular carcinoma; BC, breast cancer; TCGA, The Cancer Genome Atlas; GTEx, Genotype-Tissue Expression; GEO, Gene Expression Omnibus; GO, Gene Ontology; KEGG, Kyoto Encyclopedia of Genes and Genomes; DEGs, Identification of differentially expressed genes; OS, overall survival; HPA, Human Protein Atlas; GSEA, gene set enrichment analysis; PCA, Principal component analysis; BP, biological process; CC: cellular component; MF, molecular function.

Declarations

Acknowledgments

None.

Authors' Contributions

SW, XW and XF conceived the study and analyzed the data. LJ, ZL and TZ collected and analyzed the data. SW, ZL and MY finished experimental studies All authors drafted the article and approved the final manuscript.

Funding

This work was supported by the Major Scientific and Technological Projects for collaborative prevention and control of birth defects in Hunan Province (2019SK1010).

Availability of data and materials

The datasets analyzed in this study are available in the TCGA, GTEx and GEO databases.

Ethics approval and consent to participate

Not applicable.

Consent for publication

Not applicable.

Competing interests

The authors declare that they have no competing interests.

Author details

[1]Department of Obstetrics and Gynecology, The Second Xiangya Hospital of Central South University, Changsha, Hunan, 410011, China

References

1. Meirson T, Bomze D, Markel G. Cytoreductive Surgery for Relapsed Ovarian Cancer. The New England journal of medicine. 2022;386(9):896–7.
2. Baert T, Ferrero A, Sehouli J, O'Donnell DM, González-Martín A, Joly F, et al. The systemic treatment of recurrent ovarian cancer revisited. Annals of oncology: official journal of the European Society for Medical Oncology. 2021;32(6):710–25.
3. Saul H, Gursul D, Cassidy S, Evans G. Earlier decisions on breast and ovarian surgery reduce cancer in women at high risk. BMJ (Clinical research ed). 2022;376:o258.
4. Gusev A, Lawrenson K, Lin X, Lyra PC, Jr., Kar S, Vavra KC, et al. A transcriptome-wide association study of high-grade serous epithelial ovarian cancer identifies new susceptibility genes and splice variants. Nature genetics. 2019;51(5):815–23.
5. Kopper O, de Witte CJ, Lõhmussaar K, Valle-Inclan JE, Hami N, Kester L, et al. An organoid platform for ovarian cancer captures intra- and interpatient heterogeneity. Nature medicine. 2019;25(5):838–49.
6. Chakravarty AK, McGrail DJ, Lozanoski TM, Dunn BS, Shih DJH, Cirillo KM, et al. Biomolecular Condensation: A New Phase in Cancer Research. Cancer Discov. 2022:Of1-of13.
7. Bayo J, Fiore EJ, Dominguez LM, Real A, Malvicini M, Rizzo M, et al. A comprehensive study of epigenetic alterations in hepatocellular carcinoma identifies potential therapeutic targets. J Hepatol. 2019;71(1):78–90.
8. Jiang L, Ren L, Chen H, Pan J, Zhang Z, Kuang X, et al. NCAPG confers trastuzumab resistance via activating SRC/STAT3 signaling pathway in HER2-positive breast cancer. Cell Death Dis. 2020;11(7):547.

9. Zhang R, Ai J, Wang J, Sun C, Lu H, He A, et al. NCAPG promotes the proliferation of hepatocellular carcinoma through the CKII-dependent regulation of PTEN. Journal of translational medicine. 2022;20(1):325.
10. Goto Y, Kurozumi A, Arai T, Nohata N, Kojima S, Okato A, et al. Impact of novel miR-145-3p regulatory networks on survival in patients with castration-resistant prostate cancer. British journal of cancer. 2017;117(3):409–20.
11. Zhang N, Ng AS, Cai S, Li Q, Yang L, Kerr D. Novel therapeutic strategies: targeting epithelial-mesenchymal transition in colorectal cancer. The Lancet Oncology. 2021;22(8):e358-e68.
12. Yang D, Sun Y, Hu L, Zheng H, Ji P, Pecot CV, et al. Integrated analyses identify a master microRNA regulatory network for the mesenchymal subtype in serous ovarian cancer. Cancer cell. 2013;23(2):186–99.
13. Liu Y, Zhao R, Chi S, Zhang W, Xiao C, Zhou X, et al. UBE2C Is Upregulated by Estrogen and Promotes Epithelial-Mesenchymal Transition via p53 in Endometrial Cancer. Mol Cancer Res. 2020;18(2):204–15.
14. Chang YW, Chiu CF, Lee KY, Hong CC, Wang YY, Cheng CC, et al. CARMA3 Represses Metastasis Suppressor NME2 to Promote Lung Cancer Stemness and Metastasis. American journal of respiratory and critical care medicine. 2015;192(1):64–75.
15. Zhang W, Zhangyuan G, Wang F, Jin K, Shen H, Zhang L, et al. The zinc finger protein Miz1 suppresses liver tumorigenesis by restricting hepatocyte-driven macrophage activation and inflammation. Immunity. 2021;54(6):1168-85.e8.
16. Li Y, Xie X, Jie Z, Zhu L, Yang JY, Ko CJ, et al. DYRK1a mediates BAFF-induced noncanonical NF-κB activation to promote autoimmunity and B-cell leukemogenesis. Blood. 2021;138(23):2360–71.
17. Liuyu T, Yu K, Ye L, Zhang Z, Zhang M, Ren Y, et al. Induction of OTUD4 by viral infection promotes antiviral responses through deubiquitinating and stabilizing MAVS. Cell Res. 2019;29(1):67–79.
18. Bondong S, Kiefel H, Hielscher T, Zeimet AG, Zeillinger R, Pils D, et al. Prognostic significance of L1CAM in ovarian cancer and its role in constitutive NF-κB activation. Annals of oncology: official journal of the European Society for Medical Oncology. 2012;23(7):1795–802.
19. Qin Q, Xu Y, He T, Qin C, Xu J. Normal and disease-related biological functions of Twist1 and underlying molecular mechanisms. Cell Res. 2012;22(1):90–106.
20. Radisky DC, Bissell MJ. NF-kappaB links oestrogen receptor signalling and EMT. Nature cell biology. 2007;9(4):361–3.
21. Li H, Jin Y, Zhao Y, Li W, He Z, Zhang Q, et al. Targeted cell therapy for partial-thickness cartilage defects using membrane modified mesenchymal stem cells by transglutaminase 2. Biomaterials. 2021;275:120994.
22. Shijie L, Zhen P, Kang Q, Hua G, Qingcheng Y, Dongdong C. Deregulation of CLTC interacts with TFG, facilitating osteosarcoma via the TGF-beta and AKT/mTOR signaling pathways. Clin Transl Med. 2021;11(6):e377.

23. Kong D, Zhang Z, Chen L, Huang W, Zhang F, Wang L, et al. Curcumin blunts epithelial-mesenchymal transition of hepatocytes to alleviate hepatic fibrosis through regulating oxidative stress and autophagy. Redox Biol. 2020;36:101600.
24. Chen B, Song Y, Zhan Y, Zhou S, Ke J, Ao W, et al. Fangchinoline inhibits non-small cell lung cancer metastasis by reversing epithelial-mesenchymal transition and suppressing the cytosolic ROS-related Akt-mTOR signaling pathway. Cancer Lett. 2022;543:215783.
25. Yeung TL, Leung CS, Wong KK, Gutierrez-Hartmann A, Kwong J, Gershenson DM, et al. ELF3 is a negative regulator of epithelial-mesenchymal transition in ovarian cancer cells. Oncotarget. 2017;8(10):16951–63.
26. Mok SC, Bonome T, Vathipadiekal V, Bell A, Johnson ME, Wong KK, et al. A gene signature predictive for outcome in advanced ovarian cancer identifies a survival factor: microfibril-associated glycoprotein 2. Cancer cell. 2009;16(6):521–32.
27. Tothill RW, Tinker AV, George J, Brown R, Fox SB, Lade S, et al. Novel molecular subtypes of serous and endometrioid ovarian cancer linked to clinical outcome. Clinical cancer research: an official journal of the American Association for Cancer Research. 2008;14(16):5198–208.
28. Lisowska KM, Olbryt M, Student S, Kujawa KA, Cortez AJ, Simek K, et al. Unsupervised analysis reveals two molecular subgroups of serous ovarian cancer with distinct gene expression profiles and survival. Journal of cancer research and clinical oncology. 2016;142(6):1239–52.
29. Yeung TL, Leung CS, Wong KK, Samimi G, Thompson MS, Liu J, et al. TGF-β modulates ovarian cancer invasion by upregulating CAF-derived versican in the tumor microenvironment. Cancer research. 2013;73(16):5016–28.
30. Leek JT, Johnson WE, Parker HS, Jaffe AE, Storey JD. The sva package for removing batch effects and other unwanted variation in high-throughput experiments. Bioinformatics (Oxford, England). 2012;28(6):882–3.
31. Smyth GK, Michaud J, Scott HS. Use of within-array replicate spots for assessing differential expression in microarray experiments. Bioinformatics (Oxford, England). 2005;21(9):2067–75.
32. Yu G, Wang LG, Han Y, He QY. clusterProfiler: an R package for comparing biological themes among gene clusters. Omics: a journal of integrative biology. 2012;16(5):284–7.
33. Porter RL, Matulonis UA. Checkpoint Blockade: Not Yet NINJA Status in Ovarian Cancer. Journal of clinical oncology: official journal of the American Society of Clinical Oncology. 2021;39(33):3651–5.
34. Hitti E, Bakheet T, Al-Souhibani N, Moghrabi W, Al-Yahya S, Al-Ghamdi M, et al. Systematic Analysis of AU-Rich Element Expression in Cancer Reveals Common Functional Clusters Regulated by Key RNA-Binding Proteins. Cancer Res. 2016;76(14):4068–80.
35. Greville G, Llop E, Howard J, Madden SF, Perry AS, Peracaula R, et al. 5-AZA-dC induces epigenetic changes associated with modified glycosylation of secreted glycoproteins and increased EMT and migration in chemo-sensitive cancer cells. Clin Epigenetics. 2021;13(1):34.
36. Guo J, Jin D, Wu Y, Yang L, Du J, Gong K, et al. The miR 495-UBE2C-ABCG2/ERCC1 axis reverses cisplatin resistance by downregulating drug resistance genes in cisplatin-resistant non-small cell

lung cancer cells. EBioMedicine. 2018;35:204–21.

37. Odle RI, Walker SA, Oxley D, Kidger AM, Balmanno K, Gilley R, et al. An mTORC1-to-CDK1 Switch Maintains Autophagy Suppression during Mitosis. Mol Cell. 2020;77(2):228–40 e7.
38. Toh TB, Lim JJ, Hooi L, Rashid M, Chow EK. Targeting Jak/Stat pathway as a therapeutic strategy against SP/CD44 + tumorigenic cells in Akt/beta-catenin-driven hepatocellular carcinoma. J Hepatol. 2020;72(1):104–18.
39. Zhu M, Wu M, Bian S, Song Q, Xiao M, Huang H, et al. DNA primase subunit 1 deteriorated progression of hepatocellular carcinoma by activating AKT/mTOR signaling and UBE2C-mediated P53 ubiquitination. Cell Biosci. 2021;11(1):42.
40. Li S, Zhang J, Qian S, Wu X, Sun L, Ling T, et al. S100A8 promotes epithelial-mesenchymal transition and metastasis under TGF-beta/USF2 axis in colorectal cancer. Cancer Commun (Lond). 2021;41(2):154–70.

Tables

Table 1 is available in the Supplementary Files section.

Figures

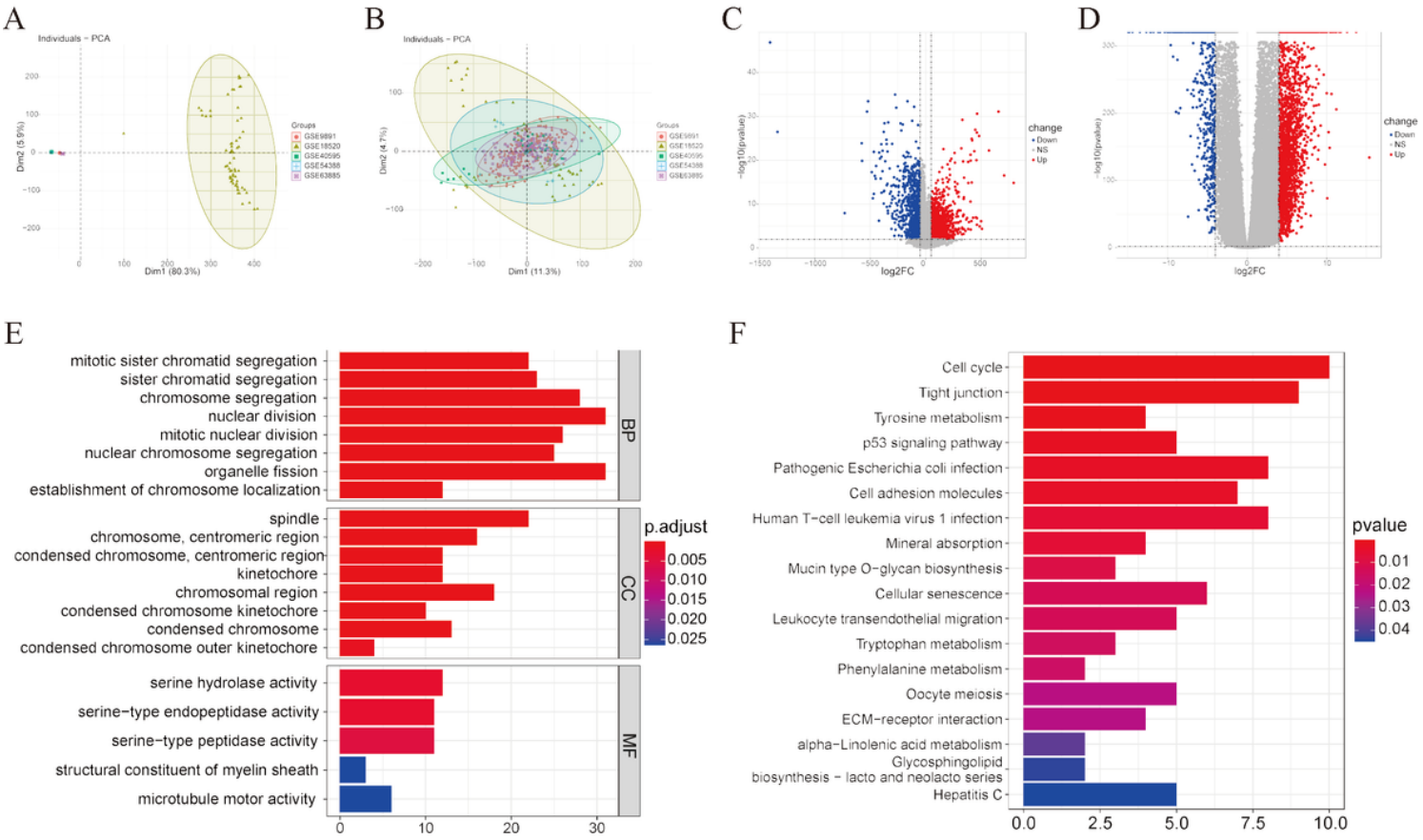

Figure 1

Identification of DEGs and functional enrichment analyses.

A. Principal component analysis (PCA) plot before batch removal in the GEO cohort. **B.** PCA plot after batch removal. **C.** Volcano plot visualizing DEGs in the GEO cohort. **D.** Volcano plot visualizing DEGs in the TCGA-GTEx cohort. **E.** Bar plot of Gene Ontology (GO) analysis. BP: biological process; CC: cellular components; MF: molecular function.

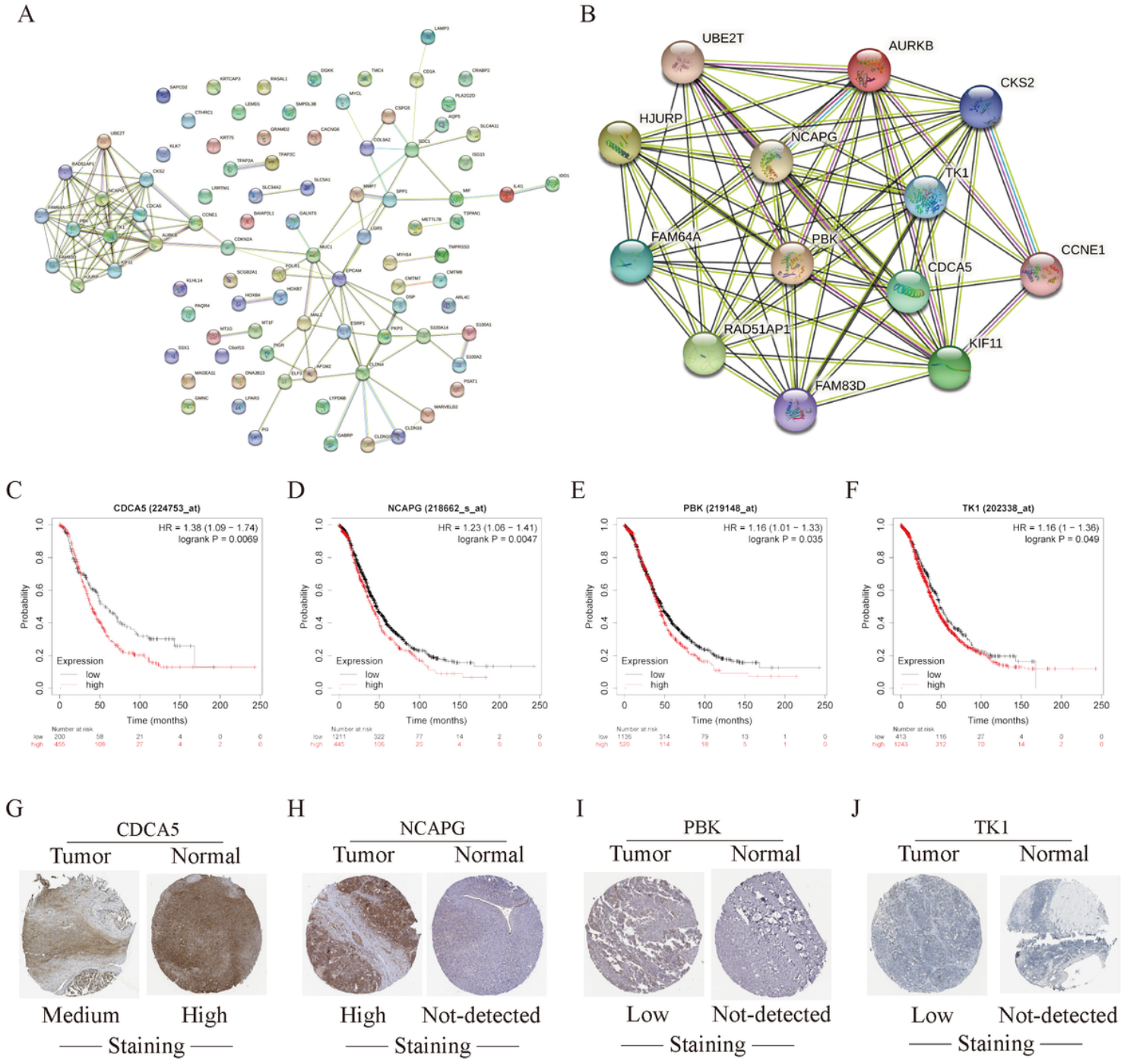

Figure 2

Screening for hub genes.

A. A PPI network constructed by 98 prognostic DEGs. **B.** A PPI network constructed by 14 central nodes from Fig. 2A. **C-F.** Kaplan–Meier plotter results of CDCA5, NCAPG, PBK and TK1. **G-J.** The protein expression levels of CDCA5, NCAPG, PBK and TK1 in OC tumor tissues and normal ovarian tissues.

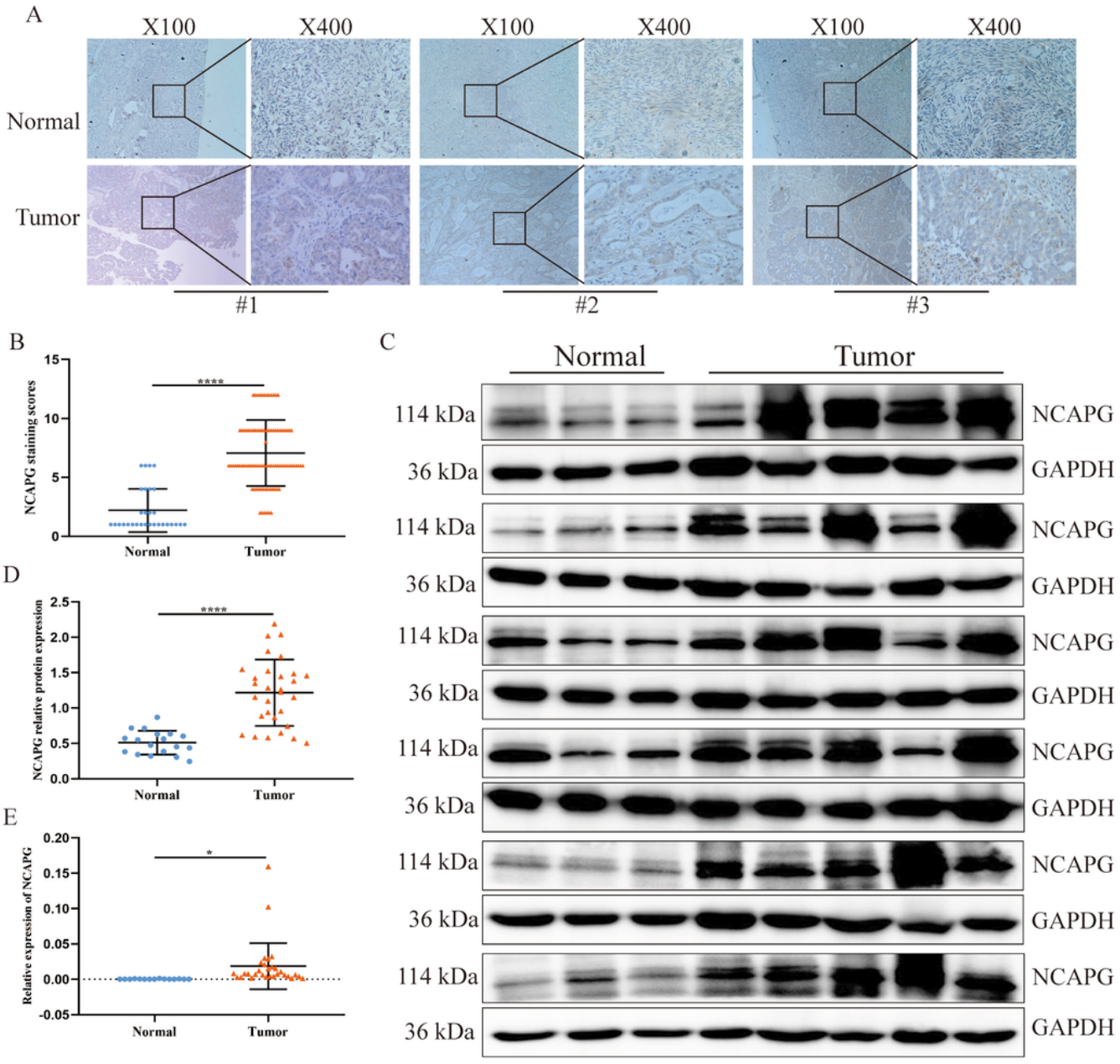

Figure 3

The expression levels of NCAPG were upregulated in EOC clinical samples

A. Representative IHC images of NCAPG staining in normal ovarian and EOC tissues. **B.** IHC staining scores of NCAPG (EOC, n=90 and NC, n=30). **C, D.** Western blot analysis of NCAPG in EOC tissues compared with normal ovarian tissues (EOC, n=30 and NC, n=18). **E.** The relative expression of NCAPG in EOC tissues compared with normal ovarian tissues (EOC, n=30 and NC, n=18). *P < 0.05, **P < 0.01, ***P < 0.001, NS, not significant.

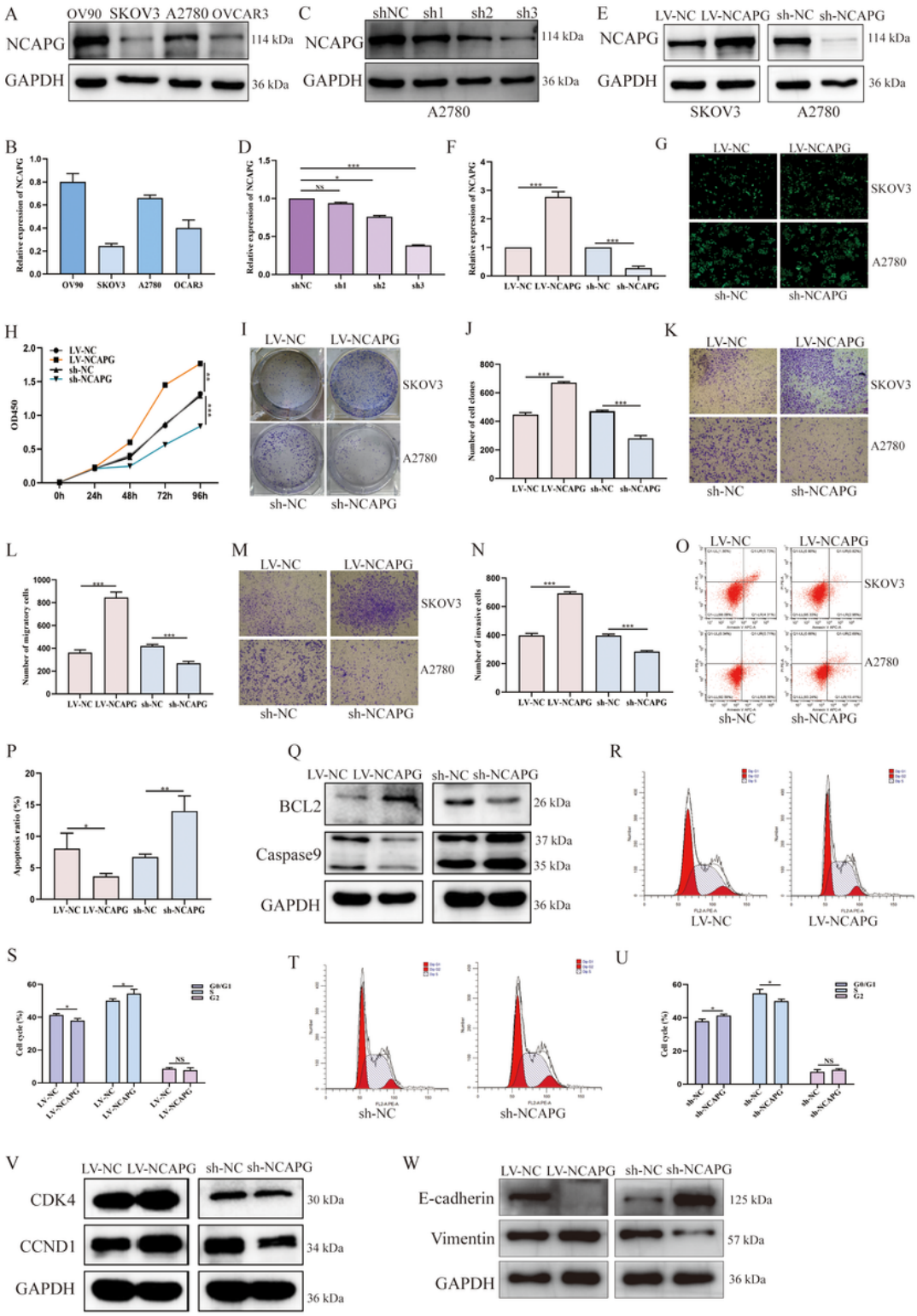

Figure 4

NCAPG promotes biological behavior, proliferation, and EMT in EOC

A, B. Western blot and qRT—PCR analysis of NCAPG expression in EOC cell lines. **C, D.** The protein and mRNA levels of NCAPG knockdown by shRNA in the A2780 cell line. **E-G.** Western blot, qRT—PCR assays, and FITC 495/519 staining (green) identified the efficiency of NCAPG knockdown or overexpression using lentiviral infection. **H.** CCK8 assay showed the proliferation of EOC cells upon NCAPG knockdown or overexpression. **I, J.** Clone formation assays were performed when the expression levels of NCAPG were changed. **K, L.** The migration ability of NCAPG knockdown or overexpression EOC cells and control cells was detected by transwell assays without Matrigel. **M, N.** The invasive ability was detected by Matrigel-coated transwells when the expression levels of NCAPG were changed in EOC cells. **O, P.** The effect of NCAPG knockdown or overexpression on the apoptosis of EOC cells was detected by flow cytometry. **Q.** Western blot analysis of apoptosis-associated protein expression upon NCAPG knockdown or overexpression in EOC cells. **R-U.** Knockdown or overexpression of NCAPG affected the cell cycle in EOC cells. **V.** Western blot analysis of cell cycle-associated protein expression upon NCAPG knockdown or overexpression in EOC cells. **W.** Western blot analysis of EMT-related indicators of NCAPG knockdown or overexpression of EOC cells. *P < 0.05, **P < 0.01, ***P < 0.001, NS, not significant.

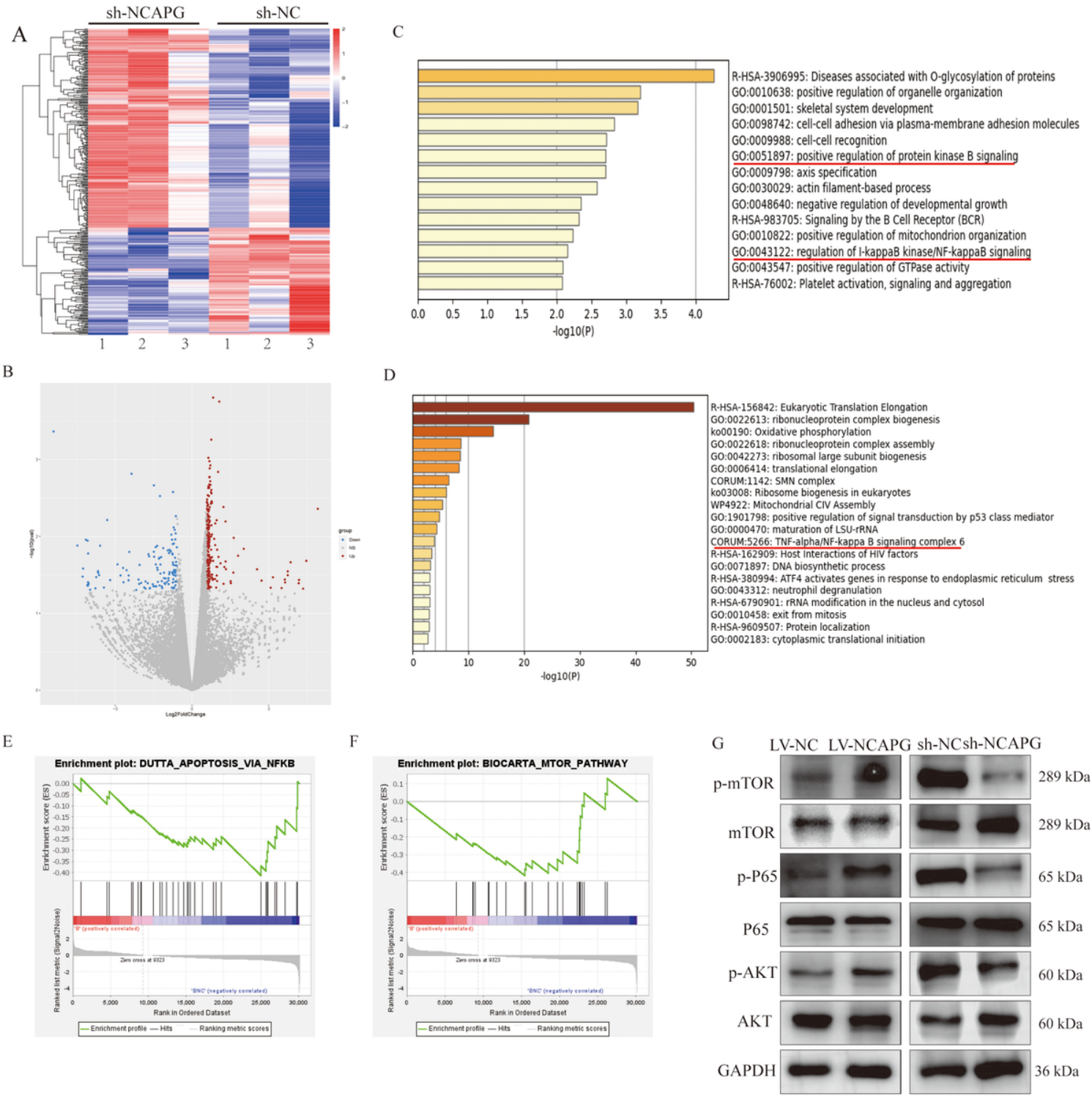

Figure 5

NCAPG promotes EMT by activating the NF-κB and AKT/mTOR pathways

A, B. Heatmap and volcano plot of differentially expressed genes from RNA-seq analysis of NCAPG knockdown and control A2780 cells. **C, D.** The differentially expressed genes in NCAPG knockdown and control cells were subjected to GO functional enrichment analysis. **E, F, G.** GSEA was used to analyze the expression levels of genes from NCAPG knockdown and control cells. **H.** The expression of proteins

associated with the signaling pathway was detected by western blotting. *P < 0.05, **P < 0.01, ***P < 0.001, NS, not significant.

Figure 6

NCAPG promotes EOC growth in vivo by activating the NF-κB and AKT/mTOR pathways

A, B. Images of xenograft tumors derived from subcutaneous implantation of SKOV3 cells and tumor growth curves of NCAPG-overexpressing and control cells in NOD SCID mice. **C, D.** Images of xenograft tumors derived from subcutaneous implantation of A2780 cells and tumor growth curves of NCAPG knockdown and control cells in NOD SCID mice. **E, F.** Ki-67 expression was analyzed by IHC in tumors with different treatments. **G, H.** The proteins associated with the signaling pathway were detected by western blotting in tumors with different treatments. *P < 0.05, **P < 0.01, ***P < 0.001, NS, not significant.

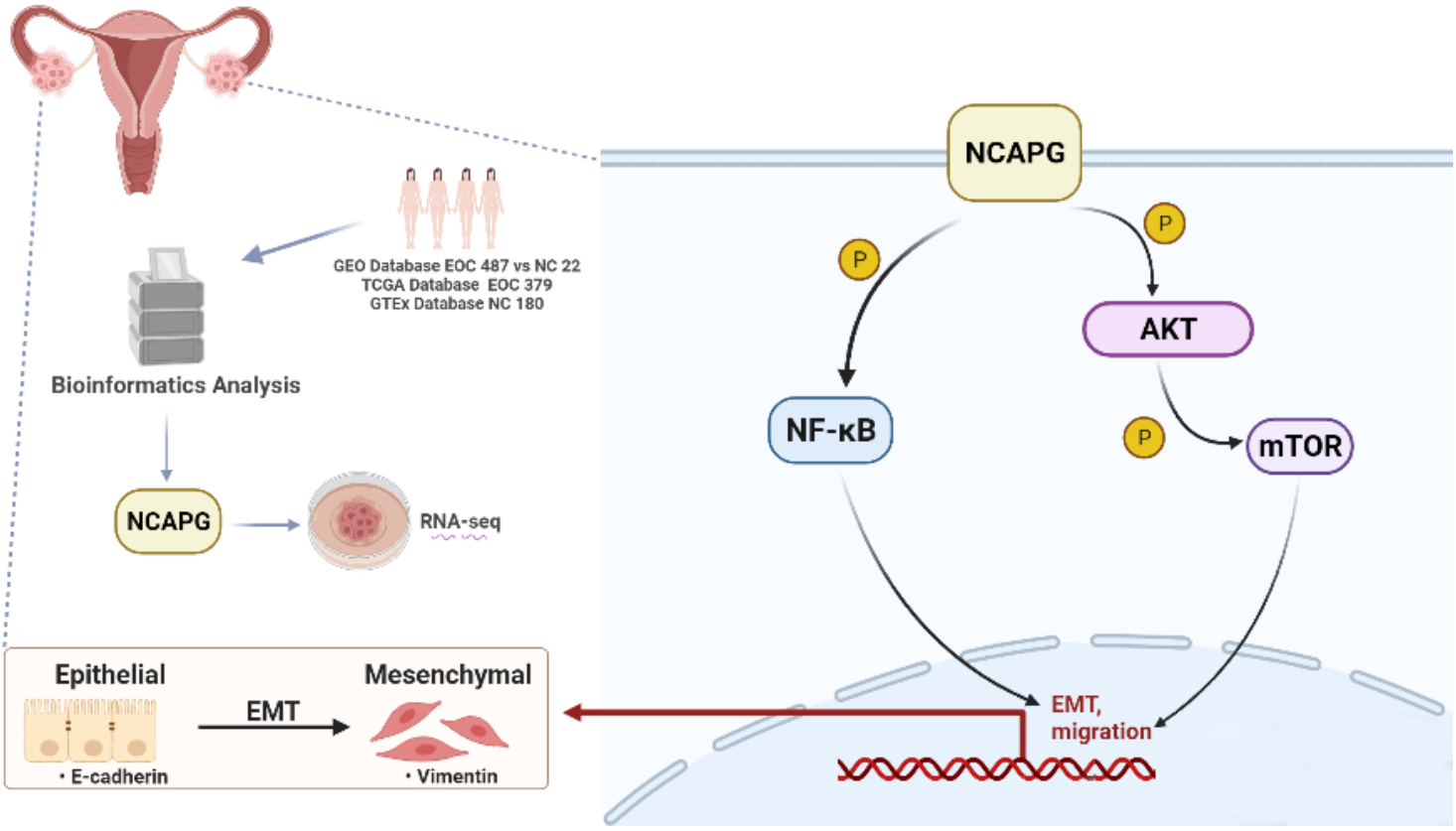

Figure 7

Graphical Abstract

Supplementary Files

This is a list of supplementary files associated with this preprint. Click to download.

- Table1.tif
- GA.png
- Supplementarymaterial.pdf